Journal of Inorganic Biochemistry 200 (2019) 110804

Contents lists available at ScienceDirect

Journal of Inorganic Biochemistry

journal homepage: www.elsevier.com/locate/jinorgbio

Structure and redox stability of [Au(III)(XˆNˆX)PR_3] complexes (X = C or N) in aqueous solution: The role of phosphine auxiliary ligand

Giset Y. Sánchez Delgado[a], Diego Paschoal[b], Marcone A.L. de Oliveira[c], Hélio F. Dos Santos[a,*]

[a] NEQC: Núcleo de Estudos em Química Computacional, Department of Chemistry, Federal University of Juiz de Fora, Campus Universitário Martelos, 36.036-900 Juiz de Fora, MG, Brazil
[b] NQTCM: Núcleo de Química Teórica e Computacional de Macaé, Polo Ajuda, Federal University of Rio de Janeiro, Campus UFRJ-Macaé, 27.971-525 Macaé, RJ, Brazil
[c] GQAQ: Grupo de Química Analítica e Quimiometria, Department of Chemistry, Federal University of Juiz de Fora, Campus Universitário Martelos, 36.036-900 Juiz de Fora, MG, Brazil

ARTICLE INFO

Keywords:
Gold complex
Phosphine
Reduction potential
Buried volume

ABSTRACT

The choice of the auxiliary ligand in Au(III) complexes is of paramount importance in tuning their reactivity and biological activity. Tertiary phosphines are one of the most used auxiliary ligands in gold compounds, due to their stereo-electronic properties that confer stability and lipophilicity to these metallodrugs. The redox stability of $[Au(III)(CˆNˆC)PR_3]^+$ (A) (CˆNˆC = 2,6-diphenylpyridine) and $[Au(III)(NˆNˆN)PR_3]^{3+}$ (NˆNˆN = 2,2′:6′,2″-terpyridine) (B) complexes (where R is the phosphine substituent groups with different steric and electronic properties) was herein investigated for a set of 41 phosphines, using the predicted standard reduction potential (ε^o) for Au(III)/Au(I) electrochemical system as reference. For the complexes A, ε^o spread over 829 mV and all values were negative, whereas for the complexes B ε^o were positive and covered a narrower range of 507 mV. The phosphines with high buried volume ($\%V_{bur} \geq 32\%$) decrease the complex stability despite being strong σ-donors. Both steric and electronic properties were used as molecular descriptors to build quantitative structure-property relationships (QSPR), which showed that the $\%V_{bur}$ plays the major role on the redox stability of the studied Au(III) complexes. For complexes B where the phosphine affects both Au(III) and Au(I) forms, the steric impact is more pronounced on the Au(I) reduced species. The electron-donating ability of phosphines is also important and plays a greater role on the redox stability of complexes B than complexes A. These outcomes are certainly useful to predict the redox stability of Au(III) complexes which, in turn, should affect their chemical reactivity against biological targets.

1. Introduction

Auranofin (AF), an Au(I) complex containing PEt_3 as auxiliary ligand, was approved by Food and Drugs Administration (FDA) in 1985 for the treatment of rheumatoid arthritis, despite its side effects [1]. In mid-80s, AF also showed to be a potent inhibitor of the growth of tumor cells in vitro with antitumor activity in vivo limited in mouse tumor models [2]. Since then, the search for promising anti-cancer gold compounds has been continuously active [3] and a large number of Au (I) and Au(III) complexes was synthesized [3–5]. Studies on the mechanism of action for both AF and $[Au(I)(PEt_3)Cl]$ complex indicated that the phosphine plays a key role to the biological activity [5]. Thus, the use of phosphines (PR_3 - R = H, alkyl, aryl, etc.) as auxiliary ligand has accompanied the synthesis of various gold complexes [5–12]. Phosphines are σ-donor and π-acceptor ligands and stabilize mainly low oxidation states of soft metal, such as Au(I), and are one of the few ligands which electronic properties can be widely modified in a systematic way by changing the R groups. Besides, they confer a lipophilic character to the compounds facilitating the cellular uptake [9,10], which is essential for improving the overall biological response [9–12].

The Au(III) complexes show instability through intracellular redox reactions, being easily reduced to Au(I) and Au(0) derivatives by cellular compounds containing thiols groups such as glutathione (GSH) [4,13]. Generally, their redox stability is improved by polydentate ligands, such as NˆN (e.g. 2,2′-bipyridine; 1,10-phenanthroline; 2-(1H-Imidazol-2-yl) pyridine; 2-(2-pyridyl)benzimidazole), NˆNˆN (e.g. 2,2′-diethylenetriamine; 2,2′:6′,2″-terpyridine; 2,6-bis(imidazol-2-yl)pyridine; 2,6-bis (benzimidazol-2-yl)pyridine), CˆN (e.g. 2-phenylpyridine; 2-phenylimidazole, 2-benzylpyridine; 2-(dimethylaminomethyl)phenyl), CˆNˆN (e.g. 6-(1,1-dimethylbenzyl)-2,2′-bipyridine), and CˆNˆC (e.g. 2,6-diphenylpyridine), porphyrins and dithiocarbamates [4,11–13]. Additionally, the choice of the auxiliary ligand in Au(III) complexes is of paramount

* Corresponding author.
E-mail address: helio.santos@ufjf.edu.br (H.F. Dos Santos).

https://doi.org/10.1016/j.jinorgbio.2019.110804
Received 28 May 2019; Received in revised form 8 August 2019; Accepted 18 August 2019
Available online 21 August 2019
0162-0134/ © 2019 Elsevier Inc. All rights reserved.

importance in tuning their reactivity and biological action [4,5,8–17]. Then, several research groups have been dedicated to the synthesis of Au (III) complexes containing PR_3 as σ-donor auxiliary ligands, mainly because they are able to stabilize the Au(I) product against reduction to Au (0) and demetalation under physiological conditions [4,11–14].

In 2006, Li and co-workers synthesized the dinuclear Au(III) complex $[(C\hat{}N\hat{}C)_2Au_2(m\text{-}dppp)](CF_3SO_3)_2$ where dppp = bis(diphenylphosphino)propane, called Au3, which showed a potent in vitro anticancer activity [11]. Afterwards, in 2013, Au3 was tested against tumor growth in animal models displaying promising activity with better results than cisplatin and doxorubicin in suppressing tumor growth [12]. Moreover, results of acute and sub-chronic toxicities examined in mice and beagle dogs were satisfactory. An important conclusion about this study was that the phosphine groups are important to the biological activity [12], with the length of the alkyl substituents in the bridging phosphine affecting the in vitro anti-cancer activities. In addition, the high stability of Au3 compared with its Pt(II) analogous was also a crucial feature accounting for its cytotoxic effect [12]. Pincer mononuclear complexes $[Au(III)(C\hat{}N\hat{}C)L]^{n+}$ where L = Cl, PR_3, Py (pyridine) and NHCs (*N*-heterocyclic carbenes) have also shown high redox stability under physiological conditions. Ka-Lei Li and coworkers showed that these complexes do not undergo easily demetalation upon treatment with reducing agent such as GSH [11,12]. Besides, mechanistic studies have shown that those Au(III) complexes are nM inhibitors of isolated Thioredoxin Reductase enzyme (TrxR) [11,12,14].

In the last two years, we have been studying Au(III)→Au(I) reduction for complexes of the type $[Au(III)(C\hat{}N\hat{}C)L]^{n+}$ through computational methods [18,19]. Our theoretical protocol was able to predict the reduction potential within ~100 mV of precision [18]. The reactivity of the complex [Au(III)(CˆNˆC)Cl] was recently studied in the presence of H_2O, CH_3SH/CH_3S^-, CH_3Se^- and 4-methylimidazole nucleophiles [19]. The results suggested that these complexes can be activated by nucleophiles available in the organism and further be reduced to Au(I) derivative. These results added to some recent experimental works [4,13,15–17], suggesting that the action mechanisms of Au(III) complexes are somehow related to their redox stability. Therefore, the auxiliary ligand in Au(III) complexes can be taken as a structural feature to tune the chemical reactivity, which, in turn, will affect the overall biological response.

In the present work, the redox stability of $[Au(III)(C\hat{}N\hat{}C)PR_3]^+$ (A) and $[Au(III)(N\hat{}N\hat{}N)PR_3]^{3+}$ (B) complexes was evaluated regarding the variation of PR_3 auxiliary ligands. The PR_3 is represented by 41 symmetric and asymmetric phosphines with equivalent (R_3 = RRR) and non-equivalent ($R_3 = R_2R'$ and RR′R″) substituents shown in Fig. 1 selected from ref. [20]. The standard reduction potential (ε^o) for Au (III) → Au(I) electrochemical system was calculated and the values discussed based on steric and electronic structural parameters. Multiple regression analysis (MRA) was also used to fit general quantitative structure-property relationship (QSPR) models, useful to predict standard reduction potential from intrinsic molecular properties.

2. Computational methods

The geometries of the Au(III), Au(I) complexes and phosphines were optimized and characterized as minimum on the potential energy surface (PES) at PBE0 density functional theory (DFT) level [21]. This functional showed to be suitable for estimation of reduction potential of Au(III) complexes [19]. The basis sets Def2-TZVP [22,23] was used for gold atom (effective core potential – ECP - for the 60 inner electrons and the triple-zeta basis set with one set of f-polarization functions for 19 valence electrons) and the 6-31 + G(2d) for the ligand atoms (hereafter abbreviated as PBE0/Def2-TZVP/6-31 + G(2d)). This same computational protocol was successfully applied for $[Au(III)(C\hat{}N\hat{}C)L]^{n+}$ complexes to predict reduction potential and represent ligand-exchange reactions [18,19].

The standard reduction potential (ε^o) for the complexes A and B of Fig. 1 was calculated in aqueous solution, based on the electrochemical cell half-reactions in relation to the standard hydrogen electrode (SHE).

$$[Au(III)(X\hat{}N\hat{}X)^nPR_3]^{3+n}_{(aq)} + 2e^- \rightarrow [Au(I)(X\hat{}N\hat{}X)^n]^{1+n}_{(aq)} + PR_{3(aq)} \quad \Delta G^o_{Au,aq} \tag{1}$$

$$2H^+_{(aq)} + 2e^- \rightarrow H_{2(g)} \quad \Delta G^o_{SHE,aq} \tag{2}$$

where X = C (n = −2) and X = N (n = 0) in Eq. (1) for complexes A and B, respectively. Indeed, for complexes B, the phosphine does not leave the coordination sphere upon reduction and the molecular formula for the product is represented as $[Au(I)(N\hat{}N\hat{}N)PR_3]^+$. The reaction Gibbs free energy ($\Delta G_{Au,\ aq}{}^o$) (at 1 M, 1 atm and 298.15 K) was calculated including the counterpoise correction for basis set superposition error (BSSE) as represented in Eq. (3) (complexes A only). The reaction solvation energy in Eq. (3) was estimated through the integral equation formalism IEFPCM, using the solvation model based on density (SMD) variation (water, ε = 78.355) [24]. This methodology was stablished after calibration of the method according to the results summarized in the Tables S1 and S2.

$$\Delta G^o_{Au.aq} = \Delta E_g + BSSE + \Delta H^o_{T,g} + \delta\Delta G_{solv} - T\Delta S \tag{3}$$

Taking the SHE electrode as reference, the potential of electrochemical cell corresponds to the potential of the standard gold electrode (Eq. (4)).

$$\varepsilon^o(Au^{3+}/Au^{1+}) = -\frac{\Delta G^o_{Au,aq}}{2} - \varepsilon^o_{(SHE),aq} \tag{4}$$

The absolute $\varepsilon_{SHE,\ aq}{}^o$ value used in Eq. (4) was 4.28 V, calculated and recommended by Isse and Gennaro in 2010 [25]. Geometries and energies were calculated using the software Gaussian 09 Rev. D01 [26]. Natural bond orbitals (NBO) and molecular orbitals analyses were performed and visualized using the graphical program ChemCraft [27]. Steric effect of PR_3 ligands on Au(III) and Au(I) complexes was represented by the percent buried volume ($\%V_{bur}$), a descriptor proposed by Nolan and Cavallo [28,29] using the web application SambVca 2.0 [30].

3. Results and discussion

3.1. Structure and redox stability of $[Au(III)(C\hat{}N\hat{}C)PR_3]^+$ complexes (A)

The Au(III) ion forms square-planar complexes likewise Pt(II) isoelectronic cation. The square coordination sphere is slightly distorted due to the asymmetry of the four ligands. The calculated structural parameters are given in Table 1 and compared to some experimental data available for $[Au(III)(C\hat{}N\hat{}C)P(Ph)_3]^+$ (A31 in Fig. 1) in ref. [11]. Only average values over all compounds are shown, with the individual data provided in Table S3. From the data in Table 1, we note that despite the broad structural dissimilarity of PR_3 in Fig. 1, the calculated parameters for the Au(III) complexes spread over a small range, usually around 1% of the average value. Moreover, the reference values are within the calculate range, except for Au—P bond which is predicted slightly longer than expected in solid state.

Phosphines are well known as strong *trans*-director ligands. The structural *trans* effect might be measured by the stretching of the metal-ligand bond *trans* to the PR_3 group, which is attributed mainly to the σ-donor electronic effect. Fig. 2a represents the Au—N bond length (*trans* to the PR_3 group) as function of energy of HOMO (ε(HOMO)) of free phosphines. We clearly see the tendency of increasing the Au—N bond length with ε(HOMO) (R^2 = 0.61), i.e., phosphines with high HOMO energy are strong σ-donor ligands and induce a pronounced *trans* effect. Complexes containing strong electron withdrawing PR_3 ligand (low ε(HOMO)) such as A40 and A21, showed short Au—N bond (~2.02 Å), whereas those with strong electron donor PR_3 ligand (high ε(HOMO)) such as A10, showed long Au—N bond (~2.05 Å). The overall *trans* effect is satisfactorily represented by ε(HOMO) parameter; however

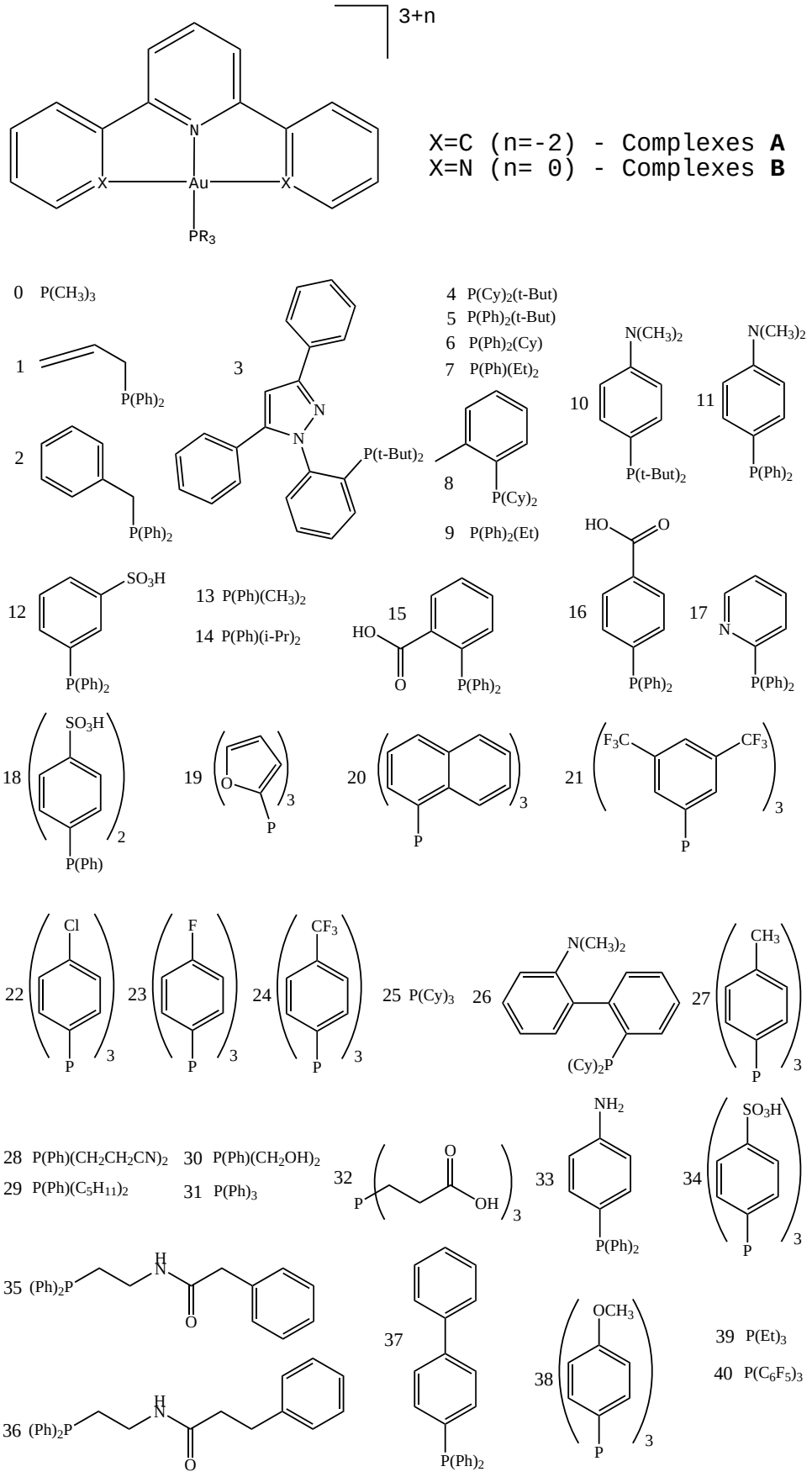

Fig. 1. Selected Au(III) complexes containing phosphine as auxiliary ligands. The phosphines were taken from ref. [20].

Table 1
Average structural parameters for the complexes $[Au(III)(C^N^C)PR_3]^+$ (A) calculated at PBE0/Def2-TZVP/6-31 + G(2d) level in gas phase.

	Average value[a]	Range of values	Reference value[b]
Au-P/Å	2.330 ± 0.033	2.303–2.395	2.297
Au-N/Å	2.032 ± 0.010	2.017–2.052	2.04
Au-C/Å	2.102 ± 0.006	2.092–2.134	2.092
C-Au-C/°	159.85 ± 1.78	154.4–169.2	161.2
N-Au-P/°	172.89 ± 3.66	162.7–178.2	176.33

[a] Average over a set of 41 structures.
[b] X-ray structure of complex A31 from ref. [11].

some outliers are noted (e.g. A4 and A10, both containing *tert*-butyl (*t*-But) group) that is in part due to the steric effect caused by bulky phosphines on the complex structure, which is not properly represented by a parameter of isolated phosphine. An attempt to improve the representation of *trans* effect by a single electronic parameter was done by defining the "total charge donating" from PR_3 to Au(C^N^C) moiety (δq_{PR_3}). The Au—N × δq_{PR_3} correlation is shown in Fig. 2b and is slightly better ($R^2 = 0.73$) than that in Fig. 2a ($R^2 = 0.61$). The δq_{PR_3} was calculated for the entire complex structure, so the electronic and steric effects of phosphine are somehow accounted for in a single molecular descriptor. In Fig. 2b we note that, the more charge is transferred from PR_3 to Au(C^N^C) moiety, more pronounced is the *trans* effect on the Au—N bond. The *trans* effect of the bulky phosphines A3, A4 and A10 (red dots in Fig. 2b) is not represented by δq_{PR_3} and the corresponding complexes were excluded from the correlation line. Fig. 2c clearly shows that the steric effect alone does not represent the *trans* effect for the series of phosphine studied, even though a trend of increasing the Au—N bond can be seen for bulky phosphines.

The interacting NBOs are shown in Fig. 3 for the simplest complex A0. Total donation energies ($\Delta E_{Lig\rightarrow Au}$) and back-donation energies ($\Delta E_{Au\rightarrow Lig}$) (Lig = PR_3 and C^N^C) were obtained by delocalization from ligand to metal and from metal to ligand, respectively. The stabilization energies $E^{(2)}$ are calculated by 2nd-order perturbation theory and given in Table S4. For most complexes, the greatest stabilization comes from [C^N^C] → Au (n → 6p) donation (Fig. 3a,b). The exceptions are the complexes A0 and A32 for which the σ → 6p donation is larger than n → 6p for C^N^C → Au (see Fig. 3c and Table S4). For the complex A0, the main contribution comes from PR_3 → Au (σ → 6p) donation (Fig. 3d). The C^N^C ligands are strong σ-donors being used for synthesis of Au(III) complexes with increased stability. On the other hand, auxiliary ligands such as tertiary phosphines have been used to guarantee stabilization of the Au(I) avoiding reduction to Au(0) form [4,12,13]. The PR_3 → Au donations (σ → 6p) and back-donations (5d → σ*) are represented by Fig. 3d,e. Electron donation is dominant for most complexes with the exception of complexes A1, A5, A30 and A33 for which Au → PR_3 (5d → σ*) back-donation has the largest $E^{(2)}$ contribution (Table S4).

The values of the reduction potentials (ε°) for the Au(III)/Au(I) electrochemical system relative to the SHE with all individual contributions to the Gibbs free energy in aqueous solution are presented in Table 2. All reduction potential values were negative and cover a broad range of 829 mV. Compounds A0, A7, A13 and A29 showed values of ε° lower than −1.0 V, being comparable to that for the derivative [Au(III)(C^N^C)Cl] (−1.07 V). The highest values of ε° were found for complexes containing electron accepting phosphines A40, A16 and A21 and for the bulky phosphines (e.g. A3-1). Experimental data for the complexes A31 and [Au(III)(C^N^C)Cl] are also available in reference [11]. Overall, by analyzing the last column of Table 2 (values in brackets), the agreement between predicted and experimental data is satisfactory, giving an error < 50 mV, with absolute values slightly overestimated. The [Au(III)(C^N^C)Cl] redox couple has non-equivalent charges (0 for reactant and − 2 for products) and, based on our previous analysis [18], the Variable-Temperature H-Atom Addition/Abstraction (VT-HAA) correction [31] must be used in order to get accurate reduction potential (see Tables 2 and S2).

Conformational change may affect the reduction processes for complexes containing bulky phosphines. This effect was assessed for the complexes A3, A26, A29, A32, A35 and A36, which can stablish distinct conformations. The optimized geometries are shown in Fig. 4 (A3 and A26) and Figs. S1–S3 (A29, A32, A35 and A36). From Figs. S1–S3 we note that in spite of the energy difference between the proposed conformers, the reduction potential does not change significantly. The greatest variation in ε° was 40 mV for A36 structure (Fig. S3). For the complexes A3 and A26 the conformational change played a more pronounced role on the redox stability of the Au(III) complexes. The conformer A3-1 contains the tpp (1,3,5-triphenyl-2-pyrazoline) substituent parallel to C^N^C ligand establishing two intramolecular π-π interactions (Fig. 4a). The rotation of −113° around the P-C(tpp) bond leads to the conformer A3-2 where the ligand is in the opposite position to the chelate group C^N^C. A weak π-π interaction is still observed and the form A3-2 is more stable than A3-1 by 2.9 kcal mol^{-1} due mainly to the relief of steric hindrance. For the complex A26 the steric hindrance is also dominant and the form A26-1, in which the bulky substituent pda (2-(phenyl)-*N*,*N*-dimethylaniline) is in opposite direction to the cyclohexyl substituent (Fig. 4b), is slightly more stable (1.4 kcal mol^{-1}). The conformational change affects the steric properties of these gold complexes. Fig. 5 shows that the forms A3-1 and A26-1 present the largest buried volume, 41.6 and 39.2%, respectively. By quoting buried volumes for each quadrant around the metal and by the use of the steric maps [29] in Fig. 5, we note that the SW quadrant is heavily hindered by the tpp ligand ($\%V_{bur}$ = 68.5 – Fig. 5a), causing a shielding of the metal center. For the conformer A3-2 the shielding decreases significantly, showing a more symmetrical distribution of steric impact ($\%V_{bur}$ = 40.2). Likewise occurs with the conformers of the complex A26; however, the shielding of gold caused by the pda ligand in A26-1 is less pronounced than found in A3-1, as shown in the NW quadrant, %

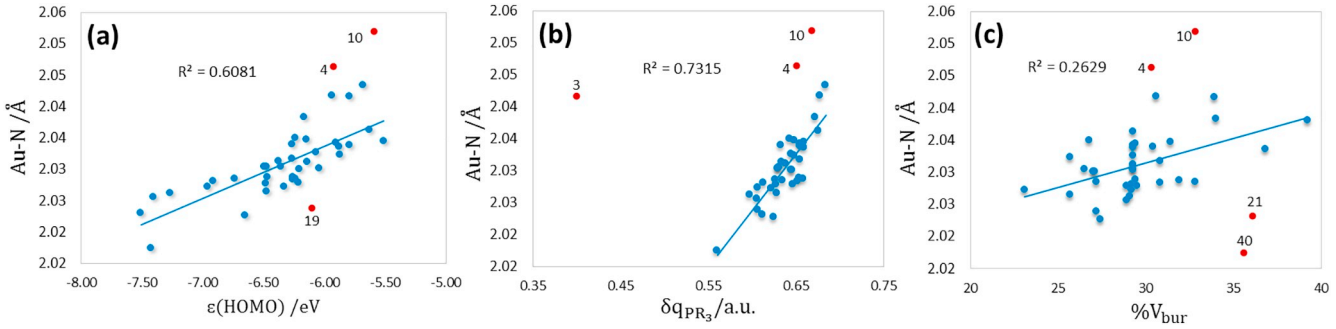

Fig. 2. Correlation between Au—N bond length and σ-donor ability of PR_3 - ε(HOMO) (a), PR_3→Au(C^N^C) total charge donating - δq_{PR_3} (b) and % buried volume - $\%V_{bur}$ (c). The complexes indicated by red dots were not included in the correlation line. (For interpretation of the references to color in this figure legend, the reader is referred to the web version of this article.)

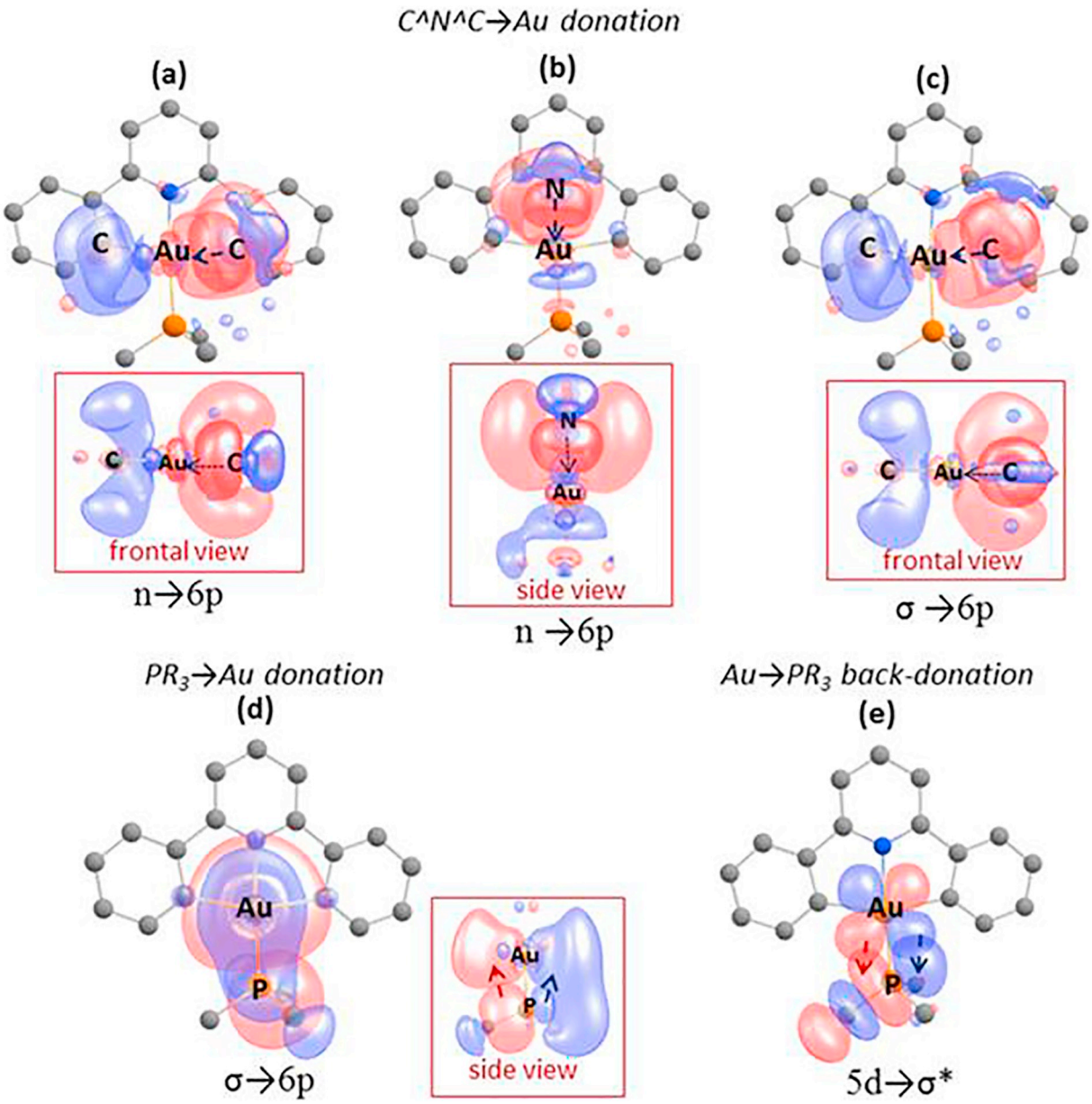

Fig. 3. Interacting natural bond orbitals (NBOs) for Au(III)···[CˆN^C] and Au(III)···$P(CH_3)_3$. LP(C)→LP*(Au) (n→6p) donation (a). LP(N)→LP*(Au) (n→6p) donation (b). BD(C−C)→LP*(Au) (σ→6p) donation (c). BD(P−C)→LP*(Au) (σ→6p) donation (d). LP(Au) → BD*(P−C) back-donation (e). The 6p orbital is slightly s, d and f polarized by about 5.4, 1.6 and 0.5% respectively in (a) and (c) and by about 3.6, 2.6 and 0.8% respectively in (b). For (d), 6p is slightly d and f polarized by about 0.2 and 0.6% respectively.

V_{bur} = 57.5 (Fig. 5b). The values of ε° in Table 2 show that A3-1 (less stable form) has a greater tendency to reduce than the A3-2 conformer with the reduction potential differing by 0.34 V. For structure A26 the reduction potential is similar for both forms, differing by 0.12 V. Overall, for isolated molecules the conformational change may have some effect on the redox stability, mainly for those complexes containing bulky phosphines. Moreover, the intermolecular interactions between these types of bulky phosphines and different environment (such as the active site of enzymes in cells), could favor one conformer and cause large variations on the reduction potential.

Electronic and steric features are relevant for studying the stability of Au(III) complexes [32]. The HOMO and LUMO energies of the free phosphines and the $\%V_{bur}$ were taken as molecular descriptors (see Table S5) and correlated to the calculated reduction potential for $[Au(III)(C\hat{}N\hat{}C)PR_3]^+$ (A) complexes. Individual linear correlations were firstly attempt as shown in Fig. 6. We found the correlation with $\%V_{bur}$ more significant (R^2 = 0.72 – Fig. 6a), which suggests an increasing of reduction potential (less stable complex) with increasing $\%V_{bur}$. Some outliers were found (e.g. A16 and A26-1) and excluded from the correlation line. The overall trend of Fig. 6a reflects the steric effect of phosphine on the charge transfer process, which requires a close ligand-metal contact so that the frontier orbitals can overlap effectively. The steric effect is clearly seen in the complexes A3, A4, A10, A20 and A26, which have high $\%V_{bur}$ and low redox stability (see values of ε° in Table 2), despite these phosphines being strong σ-donors. In Fig. 6b a poor linear trend is noted when σ-electron donating capability of phosphines - ε(HOMO) - is used as molecular descriptor, showing that pure electronic descriptor is not sufficient to represent the redox stability of Au(III) complexes, even though the qualitative trend shows that more stable complexes contain phosphines with high ε(HOMO) (strong σ-donors). It is noticeable in Fig. 2b that the behavior of the complexes containing bulky phosphines (e.g. A3, A4, A10, A20 and

Table 2
Contributions to the Gibbs free energy (in eV) and standard reduction potential (in V) calculated for $[Au(III)(C^N^C)PR_3]^+$ complexes A in aqueous solution using the PBE0-SMD/Def2-TZVP/6-31 + G(2d) level.

$[Au(III)(C^N^C)PR_3]^+$	$\Delta E_{Au,\ g}$	$\Delta H_{T,\ g}^{o}$	$T\Delta S_g$	$\delta\Delta G_{solv}$	$\Delta G_{Au,\ aq}^{o}$	ε°calc.[a]
A0	−5.44	−0.22	0.59	−0.10	−6.35	−1.11
A1	−5.42	−0.21	0.65	−0.43	−6.70	−0.93
A2	−5.41	−0.20	0.65	−0.47	−6.73	−0.92
A3-1	−6.45	−0.25	0.78	−0.53	−8.01	−0.28
A3-2	−5.96	−0.23	0.67	−0.46	−7.32	−0.62
A4	−5.91	−0.23	0.67	−0.33	−7.14	−0.71
A5	−5.59	−0.20	0.65	−0.41	−6.86	−0.85
A6	−5.43	−0.20	0.65	−0.38	−6.66	−0.95
A7	−5.35	−0.20	0.63	−0.28	−6.50	−1.05
A8	−5.67	−0.24	0.72	−0.38	−7.02	−0.77
A9	−5.38	−0.20	0.63	−0.40	−6.61	−0.98
A10	−5.69	−0.24	0.66	−0.50	−7.09	−0.74
A11	−5.23	−0.20	0.65	−0.62	−6.71	−0.93
A12	−5.68	−0.20	0.66	−0.36	−6.89	−0.84
A13	−5.39	−0.21	0.62	−0.22	−6.43	−1.06
A14	−5.68	−0.22	0.64	−0.36	−6.90	−0.83
A15	−5.59	−0.20	0.66	−1.28	−7.73	−0.83
A16	−5.59	−0.20	0.65	−0.20	−6.24	−0.45
A17	−5.48	−0.20	0.66	−0.50	−6.85	−0.85
A18	−5.94	−0.20	0.66	−0.23	−7.02	−0.77
A19	−5.70	−0.20	0.63	−0.43	−6.95	−0.80
A20	−5.81	−0.21	0.71	−0.55	−7.28	−0.64
A21	−6.48	−0.22	0.63	−0.09	−7.42	−0.57
A22	−5.71	−0.20	0.65	−0.31	−6.86	−0.85
A23	−5.65	−0.20	0.66	−0.31	−6.82	−0.87
A24	−5.97	−0.23	0.58	−0.15	−6.92	−0.82
A25	−5.43	−0.22	0.65	−0.35	−6.65	−0.96
A26-1	−5.73	−0.23	0.71	−0.55	−7.23	−0.67
A26-2	−5.59	−0.22	0.69	−0.48	−6.98	−0.79
A27	−5.30	−0.15	0.78	−0.56	−6.80	−0.88
A28	−5.98	−0.20	0.63	−0.11	−6.70	−0.93
A29	−5.28	−0.21	0.60	−0.34	−6.43	−1.07
A30	−5.49	−0.20	0.65	−0.42	−6.76	−0.90
A31	−5.46	−0.20	0.65	−0.47	−6.79	−0.89 [−0.92]
A32	−5.59	−0.21	0.68	−0.14	−6.62	−0.97
A33	−5.30	−0.20	0.66	−0.56	−6.73	−0.91
A34	−6.14	−0.18	0.65	−0.14	−7.12	−0.72
A35	−5.50	−0.20	0.65	−0.36	−6.70	−0.93
A36	−5.55	−0.20	0.65	−0.32	−6.72	−0.92
A37	−5.42	−0.20	0.68	−0.51	−6.81	−0.87
A38	−5.17	−0.21	0.67	−0.64	−6.69	−0.94
A39	−5.56	−0.22	0.63	−0.17	−6.59	−0.99
A40	−6.53	−0.20	0.71	−0.20	−7.64	−0.46
[Au(III)(C^N^C)Cl]						−1.07[b] [−1.11]

[a] Standard reduction potential (ε°) relative to SHE reference electrode calculated including the BSSE correction. The experimental values are given in brackets for complexes A31 and [Au(III)(C^N^C)Cl] [11].

[b] Calculated including BSSE and VT-HAA corrections [31]. The VT-HAA is necessary due to the unbalanced charges before and after reduction [18,31].

A26) is not represented by ε(HOMO), which is a parameter obtained for isolated phosphines. As done in Fig. 2b to represent the *trans* effect, charge donating parameters calculated from the complex structure were used (Fig. 6c,d). For the reduction potential, the effect of phosphine charge donating is better represented by the local charge variation of phosphorus atom (δq_P) ($R^2 = 0.61$, Fig. 6c) than by the total charge donating of PR_3 (δq_{PR_3}) ($R^2 = 0.34$, Fig. 6d). Fig. 6e shows the correlation ε° × ε(LUMO) and reflects the higher complex stabilization with the lower capacity to receive electrons (high ε(LUMO)), which is opposite of the effect represented by σ* occupancy involved in the 5d → σ* back-donation (Fig. 6f), the more occupied the σ* orbital in the complex, greater the tendency to reduce. Recently, Casini and coworkers carried out a study on the mechanisms of aquaporin-3 inhibition by the electronically modulated [Au(III)(1,10-phenantroline)Cl_2] complexes (Auphen) [33]. Correlations were attempt between biological response and DFT electronic and steric parameters calculated for the Auphen complexes. The correlations found were satisfactory with q (Au), dipole moment and mainly with the molecular volume, stressing the role of volume on the biological activity of Au(III) complexes.

As shown in Fig. 6, the steric and electronic molecular descriptors contribute with different weights for the redox stability of Au(III) complexes A. In order to include both parameters in a general QSPR model, multiple regression analysis (MRA) was used to fit the data for 43 structures (including both conformers of A3 and A26). The models have as independent variable the $\%V_{bur}$, δq_P, δq_{PR_3}, ε(HOMO), and ε(LUMO) and as dependent variable, the ε° vs SHE for the evaluated complexes $[Au(III)(C^N^C)PR_3]^+$ (A) considering a confidence interval of 95%. The models are shown in Table 3, which includes the coefficients of independent variables with their respectively standard errors. Regression statistics are also included for each model. Considering the standard errors in the regression coefficients, it is noted that the $\%V_{bur}$ steric descriptor presents the highest weight among the variables included. Among the electronic molecular descriptors, the δq_P charge donating is more relevant. When these two important descriptors are included in the same model (Model 5) the result is very good leading to an error lower than 100 mV for predicted values. Overall, all calculated F-values indicate that the regressions are very significant, since critical F-values are significantly lower than calculated F-values (see values in parentheses, Table 3). Besides, the maximum root mean square error is 0.119 V, corresponding to the global error equal to 14% that is acceptable for reduction potential predictions [34,35]. Lastly, it was observed by Shapiro-Wilk normality test performed in the residues a normal behavior (not shown), attesting the good quality of the modeling. The Fig. 7 shows the calculated reduction potentials and the predicted values using Model 5, with their error intervals. The complexes A1, A2, A3-2, A4, A15 and A16 are out of the confidence interval in all models (green dots in Fig. 7). The phosphines in these complexes have some intrinsic characteristics: in the complexes A3 and A4 the phosphines are strong σ-donors and have high $\%V_{bur}$, which cause a drastic increase of ε° for the corresponding gold complexes, due to the prevalence of steric effects. These phosphines contain *t*-But and cyclohexyl (Cy) substituents that, besides increasing $\%V_{bur}$, cause a great torsion on the ∠N-Au-P angles (see Fig. S4), favoring the releasing of the phosphine. On the other hand, the phosphines in complexes A15 and A16 are strong acceptors and have a $\%V_{bur} < 33\%$. Therefore, for complexes containing strong electron donor phosphines with large $\%V_{bur}$ and those with strong electron acceptor phosphines with small $\%V_{bur}$, our models fails, with the steric effects playing a major role for the reduction potential, i.e., small $\%V_{bur}$ usually favors the complex stability. The previous analysis suggests that Model 5 is applied for a $\%V_{bur}$ range between 23 and 32% that includes 33 complexes in Fig. 1 (A0, A1, A2, A4-A7, A9, A11-A14, A16-A19, A22-A25, A27-A39). Moreover, bulky phosphines such as in the complexes A4, A5, A8, A10 and A25 containing *t*-But and Cy groups lead to a high torsion of the ∠N-Au-P bond angle (see Fig. S4) and consequently facilitate their reduction. As discussed previously, some phosphines containing highly flexible bulky groups can adopt conformations that significantly increase the buried volume and consequently, destabilize the complex (e.g. A1, A2, A5 in Fig. S5), increasing the reduction potential.

3.2. Structure and redox stability of $[Au(III)(N^N^N)PR_3]^{3+}$ complexes (B)

In order to assess the effect of the multidentate ligand on the redox stability of the titled complexes, the reduction potentials were calculated and discussed for the analogues complexes $[Au(III)(N^N^N)PR_3]^{3+}$ (N^N^N = 2,2′:6′,2″-terpyridine – complex B in Fig. 1). Some structures were selected: B0, B3, B7, B9, B10-B14, B16, B19, B20-B21, B24-B26-2, B27, B29, B31, B32, B34, B38-B40 (see Fig. 1). Different from complexes A where the phosphine leaves the metal coordination sphere, for complexes B, two Au—N bonds are broken, keeping the phosphine bound to the gold center. The central pyridine and the

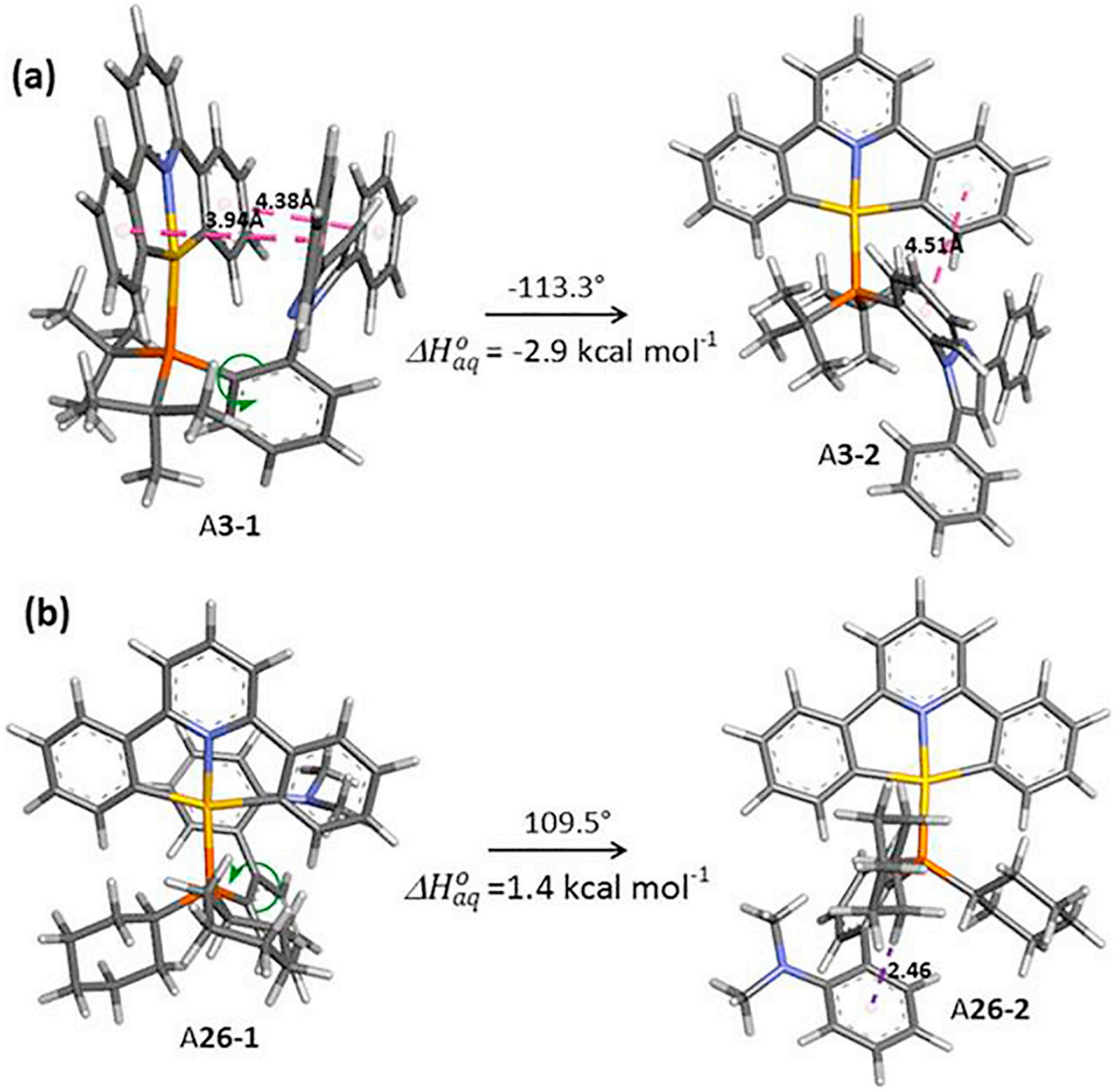

Fig. 4. Conformational isomers of complexes A3 (a) and A26 (b).

phosphine ligands are kept coordinated to gold in a linear arrangement as shown in Fig. 8a (structural parameters are provided in Table S6). Similar structural changes were evidenced during Au(III)→Au(I) intracellular reduction of complexes [Au(III)(NˆNˆN)(R-NHC)(CF_3SO_3)] (NˆNˆN = 2,6-bis(imidazol-2-yl)pyridine) [13], which are sensitive to thiols. Moreover, a fast release of the NˆNˆN ligand was observed after NˆNˆN/GSH ligand exchange reaction leading to the formation of the [Au(I)(NHC-R)(GS)] species. The modulation of R substituents on the NHC ligand caused a significant variation of the capability to inhibit TrxR and cytotoxicity against HeLa cells [13].

The steric impact of the phosphine was measured by the $\%V_{bur}$ descriptor calculated for both oxidized and reduced forms of the complexes B (see Fig. 8b). As the CˆNˆC and NˆNˆN ligands are similar in volume, the $\%V_{bur}$ values do not change much for Au(III) structures; however, it varies for Au(I) derivatives. The two-coordinate Au(I) complexes allow the PR_3 ligand to adopt a flexible conformation with less steric clashes. Consequently, the values of $\%V_{bur}$ increase for reduced species compared to the oxidized form as shown in Table S7.

As expected, due to the labiality of NˆNˆN ligand, complexes B are unstable and their reduction potentials were all positives (Table 4). We note that the trends for reduction of the complexes A and B are somehow distinct. The reduction potential spreads over 507 mV for complexes B and 829 mV for complexes A. Among the evaluated series of complexes B, the smallest reduction potential is expected for the chloride complex $[Au(III)(NˆNˆN)Cl]^{2+}$ ($\varepsilon^o = +0.57$ V); nevertheless, among the complexes with phosphine, B29 showed the greatest stabilization with reduction potential, $\varepsilon^o = +0.65$ V. The phosphine in complex B29 contains two pentyl substituents (C_5H_{11}), which do not provide a pronounced steric impact due to its high flexibility as shown by contour maps in Fig. S4 ($\%V_{bur}$ = 25.7%). This is the main feature accounting for the complex stability, regardless complexes A or B are concerning.

The NBO analysis shows that the Au(I) complexes B0, B3-2, B14, B19, B21, B24, and B39 are highly stabilized by σ-donation through the phosphorus lone pair to the 6 s orbital of metal (Fig. 9a). In fact, the LP (P) orbital of reduced complex B21 has the lowest energy (−31.23 eV)

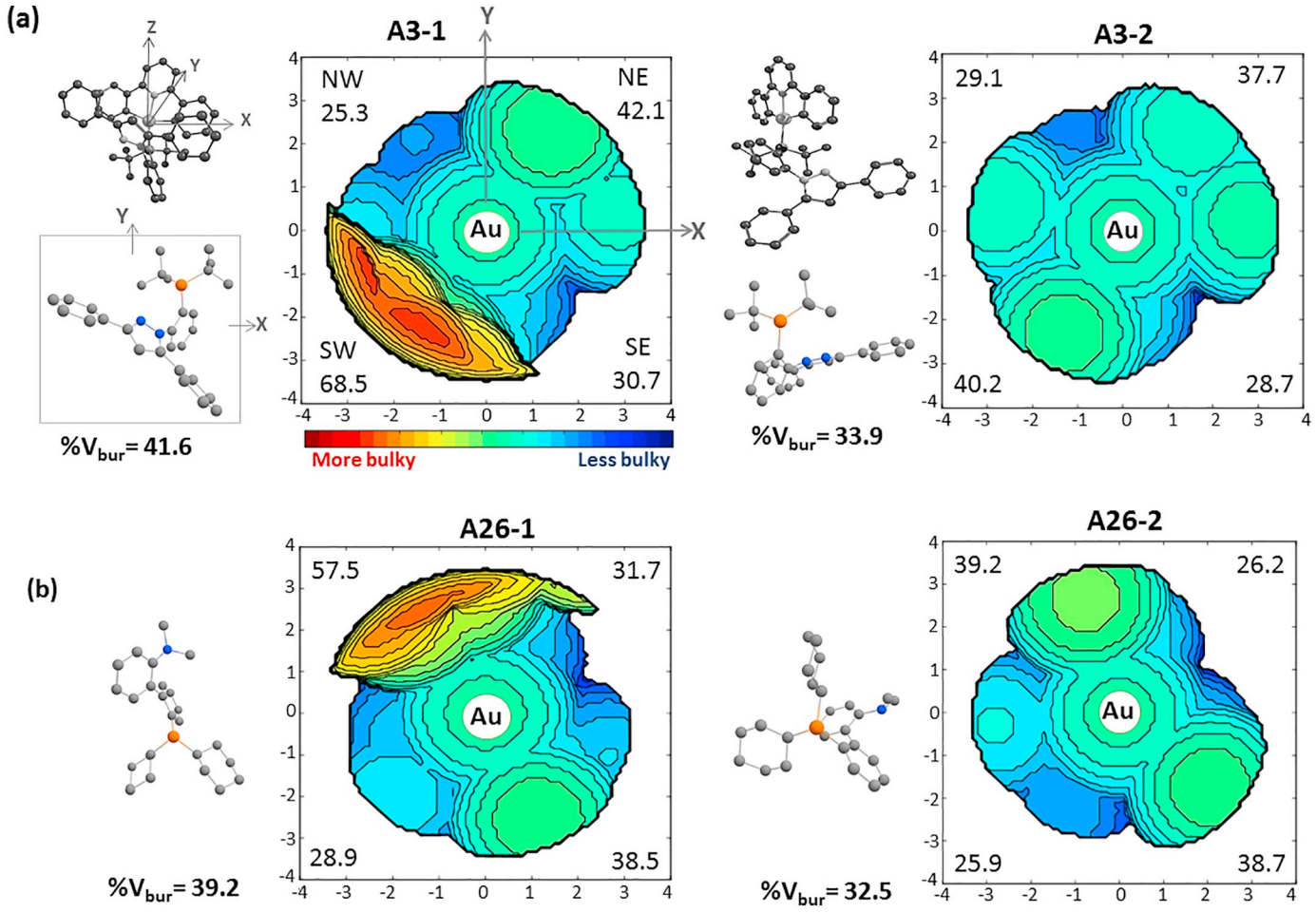

Fig. 5. Percentage of buried volume (%V_{bur}) and steric map representation for distinct conformers of complexes A3 (a) and A26 (b). The %V_{bur} is defined as the percentage of a sphere of r = 3.5 Å around the metal (mesh spacing = 0.1 Å). The hydrogen atoms were excluded.

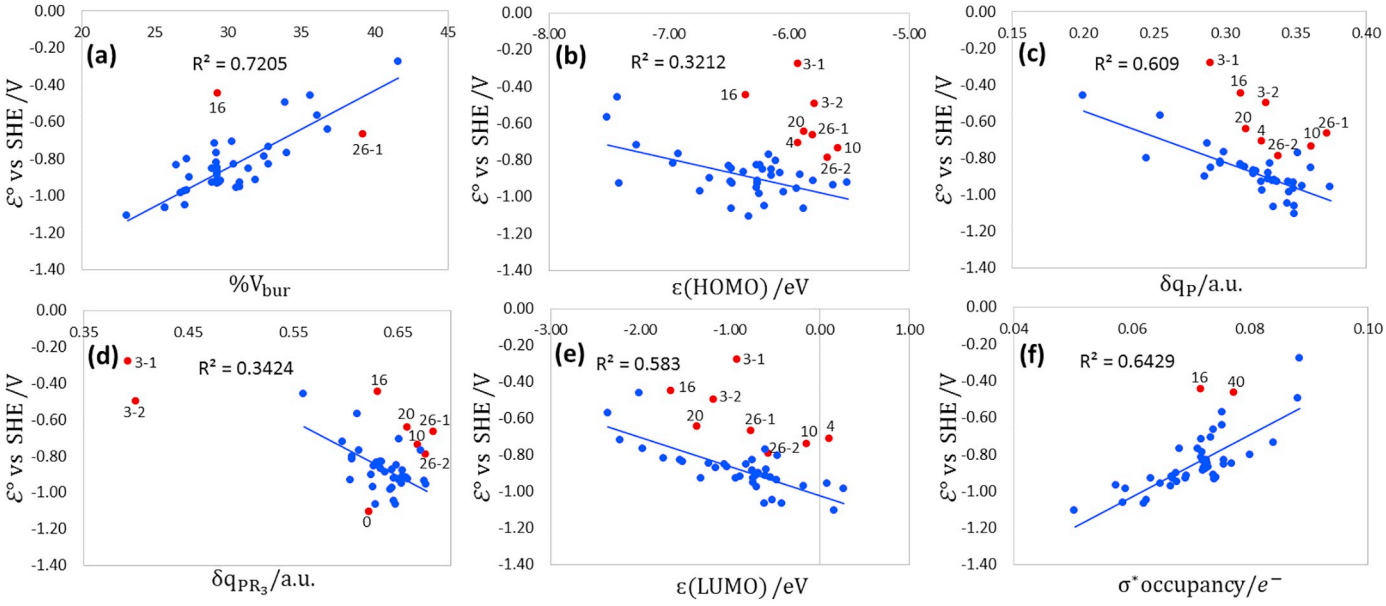

Fig. 6. Correlations between the calculated reduction potential (ε° vs SHE) of the complexes $[Au(III)(C^{\wedge}N^{\wedge}C)PR_3]^+$ (A) and the percent buried volume (%V_{bur}) (a), HOMO energy - ε(HOMO) (b), P→Au(C^N^C) charge donation (δq_P) (c), total charge donating (δq_{PR_3}) (d), LUMO energy - ε(LUMO) (e) and NBO σ* occupancy (5d → σ* back-donation) (f).

Table 3
QSPR models for prediction of the standard reduction potential (ε°/V) of complexes $[Au(III)(C^N^C)PR_3]^+$ (A). The best model is shown in bold.

	Linear regression models	R^2	SD (mV)	F value
1	ε°/V = −0.723(± 0.421) + 0.031(± 0.005)%V_{bur} + 0.079(± 0.044) ε(HOMO)/eV −0.083(± 0.037) ε(LUMO)/eV − 1.891(± 0.573) δq_P/a.u.	0.76	95.6	30.39 (2.63)
2	ε°/V = −0.781(± 0.407) + 0.027(± 0.005)%V_{bur} + 0.060(± 0.043) ε(HOMO)/eV −0.118(± 0.035) ε(LUMO)/eV-0.943(± 0.283) δq_{PR_3}/a.u.	0.76	95.2	30.7 (2.63)
3	ε°/V = −1.359(± 0.238) + 0.034(± 0.004)%V_{bur} − 0.045(± 0.032) ε(LUMO)/eV −1.664(± 0.575) δq_P/a.u.	0.74	98.3	37.3 (2.83)
4	ε°/V = −1.230(± 0.255) + 0.030(± 0.005)%V_{bur} − 0.084(± 0.026) ε(LUMO)/eV −0.908(± 0.281) δq_{PR_3}/a.u.	0.75	96.4	39.3 (2.83)
5	**ε°/V = −1.212(± 0.215) + 0.036(± 0.004)%V_{bur} − 2.146(± 0.460) δq_P/a.u.**	**0.73**	**99.4**	**53.8 (3.23)**
6	ε°/V = −1.133(± 0.282) + 0.033(± 0.005)%V_{bur} − 1.108(± 0.308) δq_{PR_3}/a.u.	0.68	107.3	43.2 (3.23)
7	ε°/V = −2.431(± 0.295) + 0.040(± 0.005)%V_{bur} − 0.063(± 0.038) ε(HOMO)/eV	0.61	119.4	31.1 (3.23)
8	ε°/V = −1.604(± 0.365) + 0.032(± 0.005)%V_{bur} + 0.047(± 0.048) ε(HOMO)/eV −0.129(± 0.039) ε(LUMO)/eV.	0.69	107.0	29.4 (2.83)
9	ε°/V = −1.940(± 0.142) + 0.034(± 0.005)%V_{bur} - 0.102(± 0.028) ε(LUMO)/eV.	0.68	107.7	43.2 (3.23)

The models used 43 structures. SD: standard deviation. Critical F-values are given in parenthesis.

compared to the others (~ −12.7 eV). This same B21 complex showed the second highest value of reduction potential among the series evaluated ($\varepsilon^o = +1.09$ V). Table S8 reports the stabilization energies for donation from phosphorus LP orbital to metal (n → 6 s). The second order estimated energy ($E^{(2)}$) for this interaction is significantly larger for complex B21 (−47.8 eV) when compared to the interactions of the other complexes, which present an $E^{(2)}$ between −12 and −16 eV (Table S8). This type of delocalization from ligand lone-pair orbital to singly occupied metal ns orbital has been observed in Au(I) complexes and being responsible for the stabilization of the complexes [36].

Due to the low polarizability of the Au(III) ion (hard acid) compared with Au(I) ion (soft acid), the Au(III)-P bond is weaker than Au(I)-P. In fact, the lone pair NBO is absent in Au(III)-complexes. Another important aspect that may influence the reduction of the complexes containing NˆNˆN ligand is that most Au(III) complexes have stronger interactions for back-donation Au → PR_3 (5d → σ*) than for donation PR_3 → Au (σ → 6p), with some exceptions for the complexes B0, B3-2, B20, B21 and B38 where the donation dominates (see Table S9). In fact, comparing the data in Tables S3 and S6 we note that the Au—P bond length is considerably smaller for complexes A than complex B. Moreover, the donation from Au—P antibonding orbital to the singly occupied metal orbital 6 s (Fig. 9b) corresponds to one of the principal delocalization in complexes B. This is also observed for complexes A, but in lower extension. From NBO analysis we also observed donation from NˆNˆN ligand (nitrogen LP) to the Au—P antibonding orbital, which show considerably greater stabilization energies than that from CˆNˆC ligand (carbon LP) to the Au—P antibonding orbital in the complexes A; however, the donation from carbon LP to the Au—C antibonding orbital provides a high stabilization to the complexes A and, in the case of complexes B, the analogous BD Au—N orbital is not formed.

In spite of small number of complexes B evaluated (24), MRA models were attempted including as independent variables the %V_{bur} for both oxidized and reduced species and the corresponding ε(HOMO) and ε(LUMO) energies for free phosphines (Table 5). The coefficients fitted show that the estimative of the reduction potential is explained in > 70% with a maximum standard error of only 81 mV. The calculated F-values indicate that the models are significant. The predicted values of the reduction potential and their corresponding error interval are represented in Fig. 10 for Model 1. According to the standard errors in the regression coefficients of the equations fitted, the %V_{bur} for the reduced species is the main parameter influencing the reduction potential for complexes B. Moreover, the contribution of the donating ability of phosphines (ε(HOMO)) also plays a role for redox stability of complexes B. For complexes B, as well as for complexes A, the steric properties play a primary role for their redox stability; nevertheless, the donating ability of phosphines is also important mainly for the stability of the Au(I) complexes B where it is determinant for redox stability. Several studies of Au(III) complexes have attempted to link the electrochemical properties with their biological effects [17,37,38].

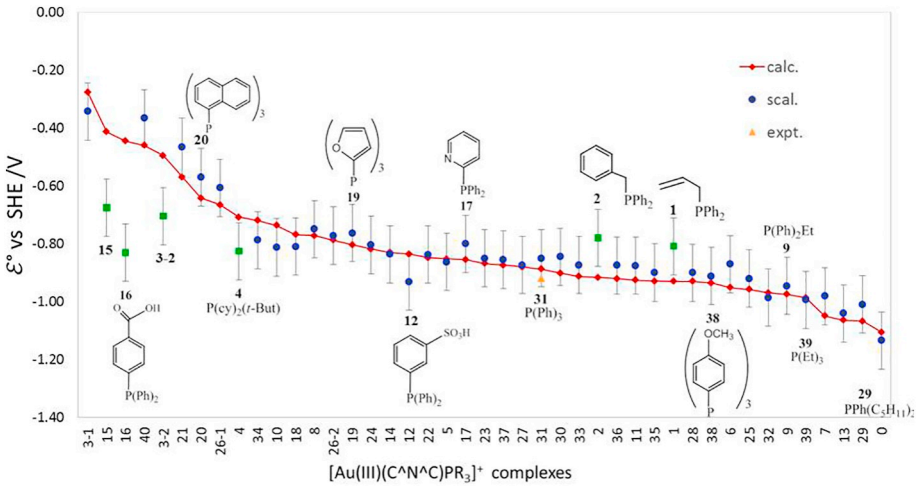

Fig. 7. Reduction trend of complexes $[Au(III)(C^N^C)PR_3]^+$ (A). The calculated PBE0 (red line) and scaled (in blue) reduction potential relative to SHE electrode are shown. Scaled values were obtained with the multiple regression Model 5. Values out of the confidence interval are highlighted in green. Experimental value for complex A31 is represented in orange color for compound A31. (For interpretation of the references to color in this figure legend, the reader is referred to the web version of this article.)

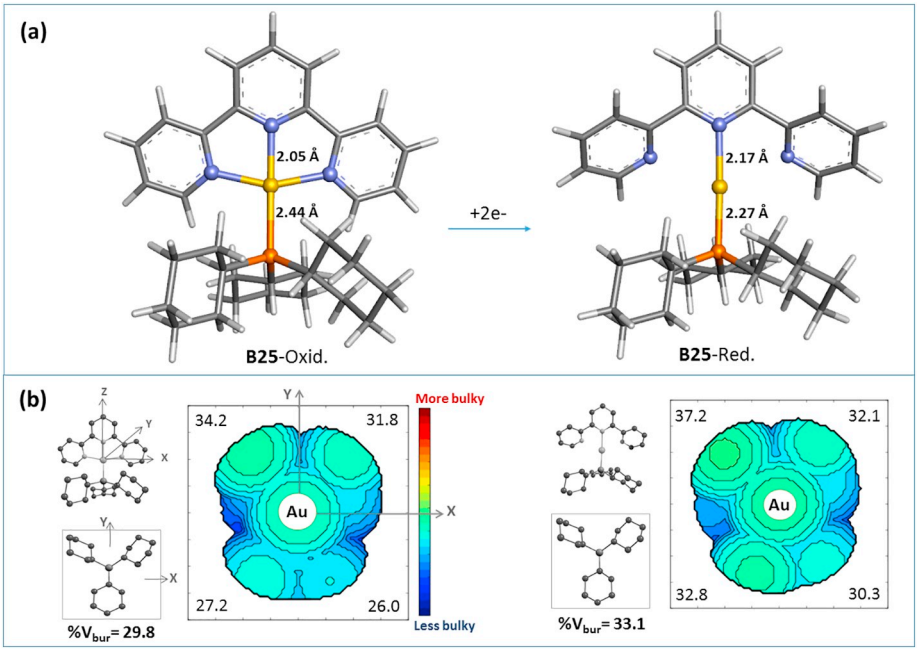

Fig. 8. PBE0 gas phase optimized structure for complex B25 in both oxidized and reduced forms (a). Percentage of buried volume ($\%V_{bur}$) and steric map representation for complex B25 (b).

Table 4
Calculated standard reduction potentials for complexes $[Au(III)(N^{\wedge}N^{\wedge}N)PR_3]^{3+}$ (B) in aqueous solution relative to the SHE electrode.

$[Au(III)(N^{\wedge}N^{\wedge}N)PR_3]^{+}$	$\Delta G_{Au,\ aq}^{o}$ (eV)	ε°calc. (V)	$[Au(III)(N^{\wedge}N^{\wedge}N)PR_3]^{+}$	$\Delta G_{Au,\ aq}^{o}$ (eV)	ε°calc.[a] (V)
B40	−10.87	+1.16	B39	−10.16	+0.80
B21	−10.75	+1.09	B19	−10.15	+0.79
B24	−10.66	+1.05	B31	−10.11	+0.77
B26-2	−10.60	+1.02	B38	−10.10	+0.77
B3-2	−10.60	+1.02	B0	−10.04	+0.76
B34	−10.51	+0.98	B27	−10.06	+0.75
B32	−10.50	+0.97	B11	−10.02	+0.73
B12	−10.48	+0.96	B9	−9.97	+0.71
B10	−10.45	+0.94	B7	−9.97	+0.71
B20	−10.4	+0.92	B13	−9.96	+0.70
B14	−10.32	+0.88	B29	−9.86	+0.65
B25	−10.21	+0.83	$[Au(III)(N^{\wedge}N^{\wedge}N)Cl]^{2+}$		+0.57 [+0.62]
B16	−10.19	+0.82			

[a] Standard reduction potential (ε°) relative to SHE reference electrode. The experimental values are given in brackets for complex $[Au(III)(N^{\wedge}N^{\wedge}N)Cl]^{2+}$ [38].

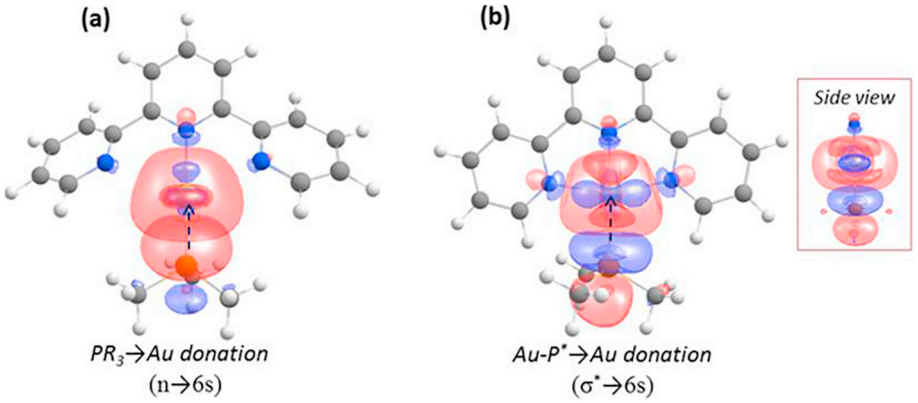

Fig. 9. Interacting natural bond orbitals (NBO) of $P(CH_3)_3\cdots Au$. LP(P) → LP*(Au) donation, n → 6 s interaction in reduced complex B0 (a); BD*(Au—P) → LP*(Au) donation, σ* → 6 s interaction in oxidized complex B0 (b).

Table 5
QSPR models for prediction of the standard reduction potential (ε°/V) of complexes $[Au(III)(N^N^N)PR_3]^{3+}$ (B). The best model is shown in bold.

	Linear regression models	R^2	SD (mV)	F value
1	**$\varepsilon^\circ/V = -0.790(\pm 0.159) - 0.022(\pm 0.010)\ \%V_{bur(Au(III))} + 0.044(\pm 0.009)\ \%V_{bur(Au(I))} - 0.150(\pm 0.024)\ \varepsilon^\circ$(HOMO)/eV**	**0.86**	**56.0**	**41.5 (3.10)**
2	$\varepsilon^\circ/V = -0.714(\pm 0.224) - 0.024(\pm 0.011)\ \%V_{bur(Au(III))} + 0.044(\pm 0.009)\ \%V_{bur(Au(I))} - 0.142(\pm 0.030)\ \varepsilon$(HOMO)/eV $- 0.013(\pm 0.025)\ \varepsilon$(LUMO)/eV	0.86	57.3	30.0 (2.89)
3	$\varepsilon^\circ/V = -0.695(\pm 0.163) + 0.025(\pm 0.003)\ \%V_{bur(Au(I))} - 0.123(\pm 0.023)\ \varepsilon$(HOMO)/eV	0.83	61.2	50.3 (3.47)
4	$\varepsilon^\circ/V = 0.581(\pm 0.235) - 0.261(\pm 0.166)\ \delta q_{PR_3-Au(III)}$/a.u. $- 0.950(\pm 0.475)\ \delta q_{PR_3-Au(I)}$/a.u. $- 0.013(\pm 0.014)\ \%V_{bur(Au(III))} + 0.042(\pm 0.013)\ \%V_{bur(Au(I))}$	0.74	79.6	13.2 (2.89)
5	$\varepsilon^\circ/V = 0.662(\pm 0.261) - 1.319(\pm 0.643)\ \delta q_{P-Au(III)}$/a.u. $- 0.157(\pm 0.590)\ \delta q_{P-Au(I)}$/a.u. $+ 0.002(\pm 0.015)\ \%V_{bur(Au(III))} + 0.021(\pm 0.013)\ \%V_{bur(Au(I))}$	0.73	80.9	12.6 (2.89)
6	$\varepsilon^\circ/V = 0.459(\pm 0.203) - 1.099(\pm 0.395)\ \delta q_{PR_3-Au(III)}$/a.u. $+ 0.027(\pm 0.004)\%V_{bur(Au(I))}$	0.70	81.3	24.0 (3.47)
7	$\varepsilon^\circ/V = 0.694(\pm 0.238) - 1.456(\pm 0.445)\ \delta q_{P-Au(III)}$/a.u. $+ 0.022(\pm 0.004)\ \%V_{bur(Au(I))}$	0.72	77.3	27.6 (3.47)

The models used 24 structures. SD: standard deviation. Critical F-values are given in parenthesis.

Generally, direct correlations between the cytotoxicity and reduction potentials are not always found [37,38]; however, when series of Au (III) compounds are evaluated against specific targets such as thiol-containing enzymes/proteins, the modulation of redox stability is quite relevant for this interaction [4,16,17,19]. This was one of the main conclusions of the recent work by Farrell et al., [17] where the results showed that a key feature that leads to the rational design of complexes $[Au(N^N^N)L]^{3+}$ (N^N^N = (dien = 2,2′-diethylenetriamine), L = R-Cyt (cytosine analogous), DMAP (4-dimethylaminopyridine) and 9-EtGua (9-etylguanine)) for interaction with the HIV nucleocapsid protein (HIV-NCp7), is the variation of their redox stability with respect to the precursor $[AuCl(dien)]^{2+}$. The NCp7-RNA interaction is interrupted in the presence of this type of gold complexes, being an important target for the treatment of AIDS [17]. Therefore, the study conducted here and the proposed QSPR models might be valuable in order to tune Au(III) redox stability by changing the auxiliary ligand. Despite the focus on phosphines, the conclusions about steric and electronic features could be extrapolated to other ligands such as NHCs.

4. Conclusions

The role of the auxiliary ligand in the stability of $[Au(III)(X^N^X)PR_3]$ (X = C,N) complexes with anticancer potential was studied using 41 PR_3 phosphines. For the complexes A, having C^N^C chelating ligand, the ε° values were negative and spread over 829 mV. This variation represents a cell energy of ~41 kcal mol^{-1} which may be highly significant for a reduction of the Au(III) complex by cellular reducing agents or for the metabolization with cellular nucleophiles. The PR_3 ligands with high $\%V_{bur}$ (32.8–41.6%) destabilize significantly the complexes, despite their strong electron σ-donating ability. Moreover, the PR_3 ligands containing the substituent *t*-But and Cy, in addition to increase the $\%V_{bur}$, cause a large torsion of the ∠N-Au-P bond angle that also contributes to facilitate the reduction of Au(III) complexes. QSPR models were proposed using ε° as dependent variable and steric and electronic descriptors depending on PR_3 ligands as independent variables. For the complexes A most of the reduction potential is represented by the steric parameters $\%V_{bur}$ with smaller contribution of charge donating of phosphine. Overall, we recommend Model 5 for complexes A with $\%V_{bur}$ in the range of 23–32%, accounting for most of phosphines commonly used as auxiliary ligand. By using Model 5 to predict reduction potential of $[Au(III)(C^N^C)PR_3]^+$ complexes the error is expected to be 0.099 V. For the complexes $[Au(III)(N^N^N)PR_3]^{3+}$ (B) all values of ε° were positive due to the labiality of the multidentate ligand N^N^N compared to C^N^C. Interestingly, the variation of the PR_3 affected the complex stability in a different way as observed for the complexes A. For complexes B, the steric impact ($\%V_{bur}$) on the reduced species was the parameter of greatest influence on the reduction potential. For complexes B, our QSPR Model 1 was statically more relevant, providing an error of only 0.056 V in the predicted reduction potential. Among the series of complexes evaluated, those containing the phosphine -$PPh(C_5H_{11})_2$ (A29 and B29) were found to stabilize the Au(III) complexes in a similar amount as Cl^-, which is often taken as reference of auxiliary ligand in stable Au(III) complexes. The long alkyl chain confers low steric hindrance and is strong σ-donors, both features contributing to stabilize the gold complex. In addition, long alkyl chain also gives the compound a more lipophilic character, being important for its activity in the cellular environment. Finally, studies of Au(III) complexes have shown that through appropriate auxiliary ligand design it is possible to develop gold complexes with potential biological activity. Interactions with

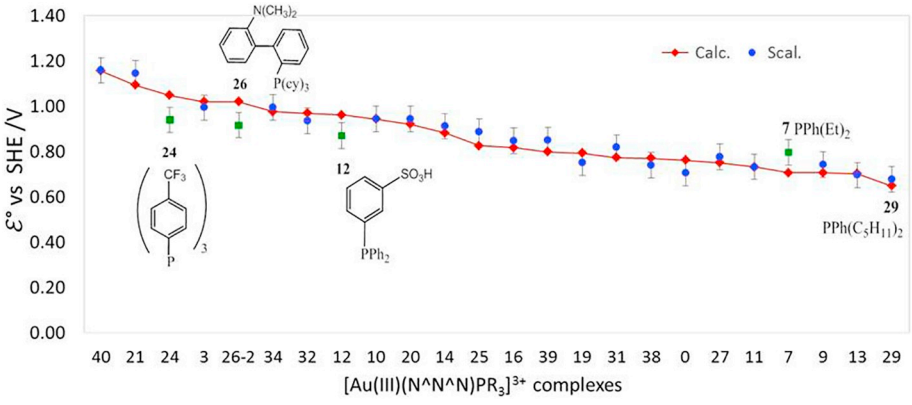

Fig. 10. Reduction trend of complexes $[Au(III)(N^N^N)PR_3]^+$ (B). The calculated PBE0 (red line) and scaled (in blue) reduction potential relative to SHE electrode are shown. Scaled values were obtained with the multiple regression Model 1. Values out of the confidence interval are highlighted in green. (For interpretation of the references to color in this figure legend, the reader is referred to the web version of this article.)

targets containing −S or −Se residues can be significantly improved through tuning the redox stability.

Abbreviations

AF	auranofin (2,3,4,6-tetra-*o*-acetyl-L-thio-β-D-glyco-pyranosato-*S*-(triethyl-phosphine)gold(I))
BSSE	basis set superposition error
CˆNˆC	2,6-diphenylpyridine
DFT	density functional theory
ECP	effective core potential
GSH	glutathione
IEFPCM	integral equation formalism polarizable continuum model
MRA	multiple regression analysis
NBO	natural bond orbital
NHC	N-heterocyclic carbene
NˆNˆN	2,2′:6′,2″-terpyridine (2,6-bis(2-pyridyl)pyridine)
PBE0	Perdew-Burke-Ernzerhof
PES	potential energy surface
QSPR	quantitative structure-property relationship
SHE	standard hydrogen electrode
SMD	Solvation Model based on solute electron Density
TrxR	Thioredoxin Reductase enzyme
VT-HAAN	Variable-Temperature H-Atom Addition/Abstraction

Acknowledgements

The authors thank CNPq and FAPEMIG for supporting this project. This study was financed in part by the Coordenação de Aperfeiçoamento de Pessoal de Nível Superior – Brasil (CAPES) – Finance Code 001.

Appendix A. Supplementary data

Supplementary data to this article can be found online at https://doi.org/10.1016/j.jinorgbio.2019.110804.

References

[1] A.E. Finkelstein, D.T. Walz, V. Batista, M. Mizraji, F. Roisman, A. Misher, Ann. Rheum. Dis. 35 (1976) 251–257.
[2] L.W. Wattenberg, Cancer Res. 45 (1985) 1–8.
[3] P.J. Sadler, R.E. Sue, Metal-Based Drugs 1 (1994) 107–144.
[4] T. Zou, C.-T. Lum, C.-N. Lok, J.-J. Zhang, C.-M. Che, Chem. Soc. Rev. 44 (2015) 8786–8801.
[5] I. Ott, Coord. Chem. Rev. 253 (2009) 1670–1681.
[6] A. Garcia, R.C. Machado, R.M. Grazul, M.T. Paz Lopes, C.C. Corrêa, H.F. Dos Santos, M.V. de Almeida, H. Silva, J. Biol. Inorg. Chem. 21 (2016) 275–292.
[7] T.T. Tavares, G.C. Azevedo, A. Garcia, A.G. Carpanez, P.M. Lewer, D. Paschoal, B.L. Müller, H.F. Dos Santos, R.C. Matos, H. Silva, R.M. Grazul, A.P.S. Fontes, Polyhedron 132 (2017) 95–104.
[8] C.K. Mirabelli, D.T. Hill, L.F. Faucette, F.L. McCabe, G.R. Girard, D.B. Bryan, B.M. Sutton, J.O. Bartus, S.T. Crooke, R.K. Johnson, J. Med. Chem. 30 (1987) 2181–2190.
[9] S.J. Berners-Price, C.K. Mirabelli, R.K. Johnson, M.R. Mattern, F.L. McCabe, L.F. Faucette, C.M. Sung, S.M. Mong, P.J. Sadler, S.T. Crooke, Cancer Res. 46 (1986) 5486–5493.
[10] S.J. Berners-Price, A. Filipovska, Metallomics 3 (2011) 863–873.
[11] C.K.-L. Li, R.W.-Y. Sun, S.C.-F. Kui, N. Zhu, C.-M. Che, Chem. Eur. J. 12 (2006) 5253–5266.
[12] R.W.-Y. Sun, C.-N. Lok, T.T.-H. Fong, C.K.-L. Li, Z.F. Yang, T. Zou, A.F.-M. Siua, C.-M. Che, Chem. Sci. 4 (2013) 1979–1988.
[13] T. Zou, C.T. Lum, S.S.Y. Chui, C.-M. Che, Angew. Chem. Int. Ed. 52 (2013) 2930–2933.
[14] S. Jürgens, V. Scalcon, N. Estrada-Ortiz, A. Folda, F. Tonolo, C. Jandl, D.L. Browne, F.E. Kühn, A. Casini, Chem. Sci. 25 (2017) 5452–5460.
[15] J. Beaton, N.P. Farrell, Inorganics 7 (2019) 1–10.
[16] M. Mora, M.C. Gimeno, Renso Visbal, Chem. Soc. Rev. 48 (2019) 447–462.
[17] C. Abbehausen, R.E. Ferraz de Paiva, R. Bjornsson, S. Quintana Gomes, Z. Du, P.P. Corbi, F. Alves Lima, N. Farrell, Inorg. Chem. 57 (2018) 218–230.
[18] G.Y. Sánchez Delgado, D. Paschoal, H.F. Dos Santos, Comput. Theor. Chem. 1108 (2017) 86–92.
[19] G.Y. Sánchez Delgado, D. Paschoal, H.F. Dos Santos, J. Biol. Inorg. Chem. 23 (2018) 1283–1293.
[20] M.K. Karver, D. Krishnamurthy, R.A. Kulkarni, N. Bottini, A.M. Barrios, J. Med. Chem. 52 (2009) 6912–6918.
[21] A.D. Becke, J. Chem. Phys. 98 (1993) 5648–5652.
[22] D. Andrae, U. Haussermann, M. Dolg, H.P. Stoll, H. Preuss, Theor. Chim. Acta 77 (1990) 123–141.
[23] F. Weigend, R. Ahlrichs, Phys. Chem. Chem. Phys. 7 (2005) 3297–3305.
[24] A.V. Marenich, C.J. Cramer, D.G. Truhlar, J. Phys. Chem. B 113 (2009) 6378–6396.
[25] A.A. Isse, A. Gennaro, J. Phys. Chem. B 114 (2010) 7894–7899.
[26] M.J. Frisch, G.W. Trucks, H.B. Schlegel, G.E. Scuseria, M.A. Robb, et al., Gaussian 09, Revision D.01, Gaussian, Inc., Wallingford CT, 2009.
[27] Chemcraft - graphical software for visualization of quantum chemistry computations, https://www.chemcraftprog.com.
[28] A. Poater, F. Ragone, S. Giudice, C. Costabile, R. Dorta, S.P. Nolan, L. Cavallo, Organometallics 27 (2008) 2679–2681.
[29] A. Poater, B. Cosenza, A. Correa, S. Giudice, F. Ragone, V. Scarano, L. Cavallo, Eur. J. Inorg. Chem. (13) (2009) 1759–1766.
[30] A. Gómez-Suárez, D.J. Nelson, S.P. Nolan, Chem. Commun. 53 (2017) 2650–2660.
[31] D. Bím, L. Rulíšek, M. Srnec, J. Phys. Chem. Lett. 7 (2016) 7–13.
[32] H.V. Huynh, Chem. Rev. 118 (2018) 9457–9492.
[33] M.N. Wenzel, A.F. Mósca, V. Graziani, B. Aikman, S.R. Thomas, A. de Almeida, J.A. Platts, N. Re, C. Coletti, A. Marrone, G. Soveral, A. Casini, Inorg. Chem. 58 (2019) 2140–2148.
[34] A.V. Marenich, J. Ho, M.L. Coote, C.J. Cramer, D.G. Truhlar, Phys. Chem. Chem. Phys. 16 (2014) 15068–15106.
[35] J. Ho, M.L. Coote, C.J. Cramer, D.G. Truhlar, B. Speiser, O. Hammerich (Eds.), Theoretical Calculation of Reduction Potentials, fifth ed., CRC Press, Boca Raton, FL, 2013(Ch).
[36] F.L. Pašteka, T. Rajský, M. Urban, J. Phys. Chem. A 117 (2013) 4472–4485.
[37] A. de Almeida, A.F. Mósca, D. Wragg, M. Wenzel, P. Kavanagh, G. Barone, S. Leoni, G. Soveral, A. Casini, Chem. Commun. 53 (2017) 3830–3833.
[38] L. Messori, F. Abbate, G. Marcon, P. Orioli, M. Fontani, E. Mini, T. Mazzei, S. Carotti, T. O'Connell, P. Zanello, J. Med. Chem. 43 (2000) 3541–3548.